Studies of Flatness of LiFi Channel for IEEE 802.11bb

Ardimas Andi Purwita and Harald Haas
School of Engineering, Institute for Digital Communications, LiFi R&D Centre, The University of Edinburgh
E-mail: {a.purwita, h.haas}@ed.ac.uk

***Abstract*— A task group named IEEE 802.11 Light Communications Amendment - Task Group "bb" (TGbb) was established in July 2018. By bringing light-fidelity (LiFi) technology into the WiFi ecosystem, LiFi can take advantage of the globally recognized WiFi brand, while also improving its capability due to the fact that LiFi does not interfere with WiFi. Early discussions in the task group focused on the physical (PHY) layer. There are two major proposals for the PHY layer. The first one is to use the existing IEEE 802.11 chipsets with LiFi analog front-ends. This is done by means of the frequency up and down-conversions and adding a DC bias. The second proposal is to redefine a whole PHY layer and optimize it by means of adopting adaptive bit loading in order to combat the low-pass filter characteristics of the non-line-of-sight wireless optical channels. Each approach has advantages in terms of the low-entry barrier to the mass market and better performance, respectively. The root question in determining the common mode PHY between the two approaches is how frequent LiFi encounters flat channels. That is, if the channel is flat, then the gain of the adaptive bit loading is not significant. Therefore, this paper aims to investigate the flatness of many samples from the reference channel models defined in the TGbb. We find that the majority of the channels are flat if the signal bandwidth is 20 MHz.**

***Index Terms*—LiFi, IEEE 802.11bb, flatness test.**

I. Introduction

In the latest Cisco Visual Networking Index [1], global mobile data traffic has doubled in 2017 compared to that in 2016, and it is predicted to increase seven-fold by 2022. At this rate, we will enter the mobile zettabyte era, where the annual global mobile data traffic will reach almost 10^3 exabytes $\left(10^9 \text{ gigabytes}\right)$ by 2022. From this traffic, 54% (13.4 exabytes/month) from the total mobile data traffic in 2017 was offloaded to fixed networks including WiFi networks. This number is predicted to increase to 59% (111.4 exabytes/month) by 2022. From the total mobile data traffic, WiFi alone will handle more than half of the total internet protocol (IP) traffic (51%) by 2022. This shows the significance of WiFi's role in future wireless communication technologies.

One of the approaches to keep up with such demands is to utilize higher spectrum, e.g., WiGig which is also known as the 60 GHz WiFi. Going further to higher frequency, the optical spectrum can also be utilized. In July 2018, a task group named IEEE 802.11 Light Communications Amendment - Task Group "bb" (TGbb) [2] was established to bring light fidelity (LiFi) [3] technology into the IEEE 802.11 ecosystem. LiFi can offer more secure connections [4] and a higher data rate per area [5]. In addition, with a well-designed load balancing scheme, LiFi can help to offload traffic from WiFi and potentially increase the throughput [6].

There are also other existing optical wireless communications' standards, e.g., the IEEE 802.15.7 [7], the IEEE 802.15.13 [8], or the International Telecommunication Union - Telecommunication Standardization Sector (ITU-T) G.9991 (also known as G.vlc) [9]. The main difference between IEEE 802.11bb and the existing standards is that the TGbb mainly focuses on delivering a mobile and networked solution of light-based communications, i.e., LiFi [3]. In addition, the TGbb specifies a few modifications to the IEEE 802.11 media access control (MAC) layer so that it can enable the co-existence of both WiFi and LiFi. Therefore, IEEE 802.11bb can leverage the globally recognized WiFi brand, and has a low barrier to entry.

Regarding the physical (PHY) layer, the details are still under discussion at the time of writing. However, a general consensus among TGbb members is to use an orthogonal frequency-division multiplexing (OFDM)-based system. There are two main proposals for the common mode mandatory physical (PHY) layer for TGbb, i.e., (i) shifting the center frequency of the output signal of existing IEEE 802.11 chipsets, or (ii) to use the PHY layer from ITU-T G.9991 [9]. For ease of reference, let us term the former proposal as *the existing PHY for light communications (LC)*, and the latter proposal as *the LC-optimized PHY*. It is optimal due to the use of adaptive bit loading in G.vlc in order to combat the low-pass filter characteristics of the non-line-of-sight channel of wireless optical channels [10]. The key advantage of using the existing PHY for LC is that it requires the least amount of changes to the existing WiFi silicon. The hope is that this will significantly reduce any barriers to entry. The main changes are in the analog front-end, which includes upconverting and downconverting the center frequency and the DC bias.

Contributions: In this paper, we analyze the potential performance losses when using the existing 802.11ax PHY layer for 802.11bb. Then, the flatness of the wireless optical channel is investigated. It is widely known that the gain of adaptive bit loading is not significant if the channel is flat. In addition, adopting the adaptive bit loading for a flat channel is also a waste of resources, e.g., mainly due to the delay of transmitting the channel state information to access points.

Other LiFi-related literature that discuss the use of the up or down conversion to obtain a real signal is commonly found in experimental works as in [11], [12]. The main motivation of

978-1-7281-3106-1/20/$31.00 ©2020 IEEE

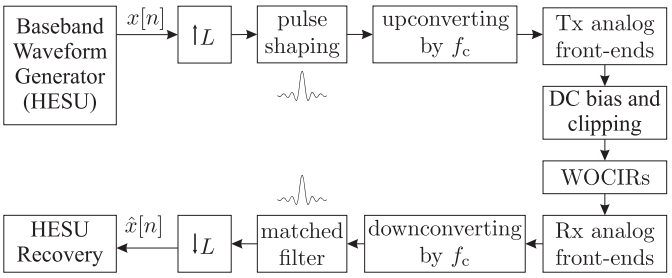

Fig. 1. System model. L denotes samples-per-symbol factor, f_c denotes the center frequency of passband signal and WOCIRs denotes the wireless optical CIRs.

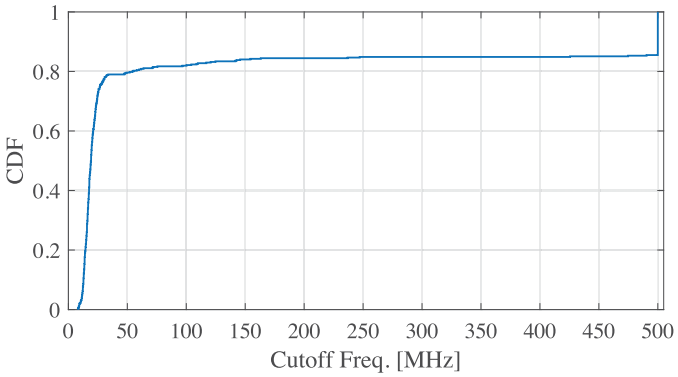

Fig. 2. CDF of the 3-dB electrical cutoff frequency of CIRs in the dataset [18] under the folders named '`individual`' and '`optical`', which have 476 samples of CIRs. Note that if the 3-dB cutoff frequency is not detected within [0,500) MHz, then it will be assigned to 500 MHz due to the sampling time equal to 1 ns.

using existing radio frequency transmission systems is similar, i.e., for more rapid development. Even though this approach is very atypical compared to the common method that applies the Hermitian symmetry as in [13], our work has merit considering the ongoing work in the TGbb, which in the future might affect the direction of research in LiFi, e.g., [14].

In Section II, the system model is provided. As the results of the flatness test highly depend on the center frequency after the upconversion, we will discuss this in Section III. The flatness test will be discussed in Section IV. Results and discussions will be provided in Section V. Section VI concludes this paper.

II. System Model

In this paper, we assume that the output signal follows the specifications defined by IEEE 802.11ax [15]. Particularly, we use an OFDM waveform that complies with the high-efficiency single-user (HESU) format. Based on [16], the main principle of the existing PHY for LC follows the ordinary passband transmission as depicted in Fig. 1. First, without loss of generality, we assume that the output signal from the existing chipsets is baseband. Then, upsampling is carried out upto 1 GSa/s and followed by pulse shaping that uses a root-raised-cosine filter. The center frequency after the upconversion is denoted by f_c. Based on [17], the transmitter front-end is modeled by a bandpass filter with the cutoff frequencies of 260 kHz and 234 MHz and the passband gain of -23.17 dB. The receiver front-end is also modeled by a bandpass filter with the cutoff frequencies of 48 kHz and 258 MHz and the passband gain of 4.6 dB. In this paper, we use the publicly-available dataset of wireless optical channel impulse responses (CIRs) that has been agreed by the TGbb [18], [19].

The TGbb has provided many samples of wireless optical channels for different scenarios in [18], [19]. The samples of CIRs are generated by using Zemax® with the sampling time of 1 ns. There are 6 scenarios, i.e.,: (i) an empty room, (ii) an enterprise-conference room, (iii) an enterprise-office room, (iv) a hospital ward, (v) an industrial environment and (vi) a residential room. Instead of random choices, the configurations of each scenario are chosen such that they are representative for typical LiFi use cases. The dataset is also organized based on the inclusion of a light emitting diode (LED) model, which has a modulation bandwidth of 20 MHz. Folders that contain those samples are named as '`individual`' [19]. In addition, folders named with '`overall`' contain aggregate CIRs that are obtained by summing CIRs from all LEDs. In this paper, we are only interested in the samples that exclude the LED model defined in [19] and the aggregate CIRs. The reason for this is that we use the LED model defined in [17] and focus on the single-input and single-output case. In terms of the scenarios, the enterprise-conference room, the hospital ward, the industrial environment and the residential room are considered. In total, we only use 476 out of 2,446 samples in the dataset. Let us draw a simple statistic from the dataset, e.g., the electrical 3-dB cutoff frequency as depicted in Fig. 2. There are 69 out of 476 samples (14.5%) that have a cutoff frequency of 500 MHz. This can later serve as a lower bound for the flatness test.

III. Center Frequency

Due to the low-pass filter characteristic of the non-line-of-sight channel [10], the flatness results depend on the region over which the upconverted signal occupies, which further depends on the center frequency. Rather than testing the flatness of channels with arbitrary values of center frequency, we aim to find an optimal center frequency in this paper. This section will be divided into three subsections. In subsection A, the trade-off in choosing a high and a low center frequency will be explained. The use of an error vector magnitude (EVM) test to find the optimal center frequency will be detailed in subsection B. Results of the optimal center frequency are given in subsection C.

A. Trade-off

A general spectral mask with the HESU format is shown in Fig. 3 with a signal bandwidth denoted by B, where $B \in \{20, 40, 80, 160\}$ MHz [15]. Now, let us investigate the effect of varying the center frequency with $B = 20$ MHz over the additive white Gaussian noise (AWGN) channels, i.e., the

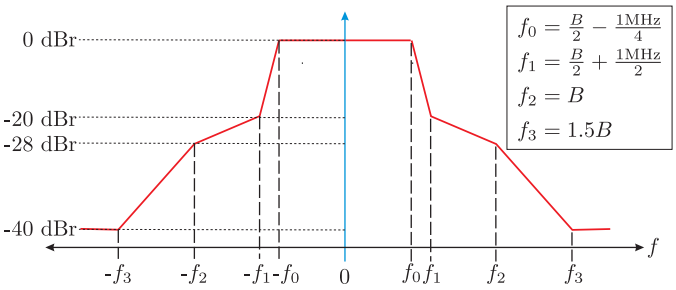

Fig. 3. The spectral mask of the OFDM waveform with the HESU format [15]. B denotes the signal bandwidth, where $B \in \{20, 40, 80, 160\}$ MHz.

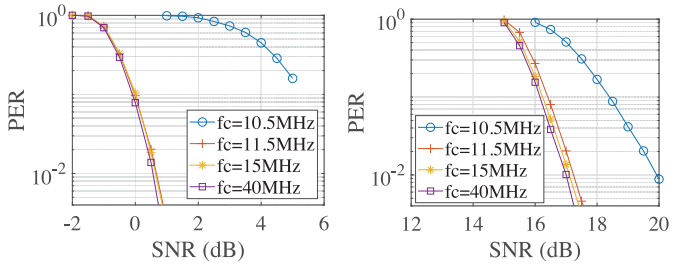

(a) MCS=0 (b) MCS=6

Fig. 4. PER vs SNR with AWGN channels for $B = 20$ MHz.

wireless optical CIR is a unit impulse. With $B = 20$ MHz, we have:

$$f_0 = 9.75 \text{ MHz}, f_1 = 10.5 \text{ MHz},$$
$$f_2 = 20 \text{ MHz and } f_3 = 30 \text{ MHz}.$$

In this case, it can be shown in Fig. 4 that as the center frequency moves further away from the DC frequency, the error performance improves. This is because a system with a higher center frequency is more resistant to spectral leakage due to aliasing near the DC frequency, which is shown in Fig. 5.

Now, we will show the trade-off of choosing a low and high center frequency by considering a frequency-selective channel, e.g., a CIR from the following folder in the dataset [18]:

`'simulation scenario enterprise-conference room/individual cirs/optical cirs/S3/D1/'`.

Note that this sample is one of the suggested samples in the methodology document [16]. This channel is also a clear example of a wireless optical channel that has the low-pass filter characteristic as shown in Fig. 6(a). Fig. 6(b) shows the trade-off. That is, choosing a higher center frequency makes the receiver more resistant to the spectral leakage. However, due to the low pass filter characteristic of the non-line-of-sight wireless optical channels, the path loss is worse, which favors a lower center frequency.

B. EVM Test

In finding the optimal center frequency, we can run the packet error ratio (PER) simulations for all selected CIRs. However, this approach is very time consuming. Therefore,

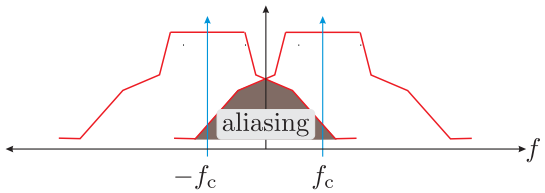

Fig. 5. Aliasing due to the spectral leakage.

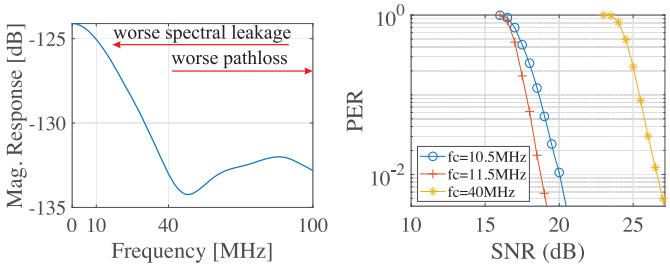

(a) (b)

Fig. 6. (a) The magnitude response of CIR from `'simulation scenario enterprise-conference room/individual cirs/optical cirs/S3/D1/Run1.mat'`. (b) The corresponding PER vs SNR with different center frequencies with $B = 20$ MHz.

in this paper, we use the EVM test. The EVM is the vector difference between the reference constellation symbols and the received constellation symbols. Hence, the EVM values can be used to predict the error performance.

We refer to [15, Table 28-46] for the upper limits of acceptable EVM values. The table is summarized in Table I for different modulation and coding scheme (MCS) index values. The procedure of the EVM test is also detailed in [15]. That is, all training fields must be used to perform frequency and timing offset corrections and equalization. The output of the equalization is used to measure the EVM. An EVM test is a success if the measured EVM is less than or equal to the corresponding upper limit.

Other than the frequency-selectivity due to the wireless optical channels, an additional impairment is added in this paper. Based on the TGbb requirement and following [20], instantaneous shot noise is also considered. Shot noise is typically present if avalanche photodiodes are used, or it comes from ambient light sources, for example, sunlight, incandescent or fluorescent lamps [21], [22]. In this sense, the EVM can be used as a predictor at high signal-to-noise ratio (SNR) when the system is limited by the frequency-selective channels and shot noise.

Measuring the EVM values using the channel depicted in Fig. 6(a) with $B = 20$ MHz and $f_c \in \{10.5, 11.5, 40\}$ MHz, we obtain the EVM values of -26.43 dB, -28.12 dB and -25.07 dB, respectively. From these values, it can be predicted that the error performance result with $f_c = 11.5$ MHz is the best, and that with $f_c = 40$ MHz is the worst. Indeed, the PER vs. SNR curves in Fig. 6(b) are consistent with our hypothesis.

C. Results and Discussions on the Optimal Center Frequency

TABLE I. Upper limits of acceptable EVM values for HESU format [15, Table 28-46].

MCS index	Modulation	Coding rate	Upper limits of acceptable EVM values in dB
0	BPSK	1/2	-5
1	QPSK	1/2	-10
2	QPSK	3/4	-13
3	16-QAM	1/2	-16
4	16-QAM	3/4	-19
5	64-QAM	2/3	-22
6	64-QAM	3/4	-25
7	64-QAM	5/6	-27
8	256-QAM	3/4	-30
9	256-QAM	5/6	-32
10	1024-QAM	3/4	-35
11	1024-QAM	5/6	-35

Based on the previous observation, we can formulate the following optimization problems:

$$\text{Case 1: } f_{\text{c}}^{*} = \underset{\substack{f_{\text{c}}\in\mathcal{F}_1,\forall\text{MCS},\forall\text{CIR}\\ \text{s.t. } E\leq\text{EVM}_{\text{up\_lim}}}}{\arg\min} \quad E, \quad \forall B, \tag{1}$$

$$\text{Case 2: } f_{\text{c}}^{*} = \underset{\substack{f_{\text{c}}\in\mathcal{F}_2,\forall\text{MCS},\forall\text{CIR},\forall B\\ \text{s.t. } E\leq\text{EVM}_{\text{up\_lim}}}}{\arg\min} \quad E, \tag{2}$$

$$\text{Case 3: } f_{\text{c}}^{*} = \underset{\substack{f_{\text{c}}\in\mathcal{F}_2,\forall\text{MCS},\forall\text{CIR},B=160\text{MHz}\\ \text{s.t. } E\leq\text{EVM}_{\text{up\_lim}}}}{\arg\min} \quad E, \tag{3}$$

where $\mathcal{F}$ is a countably finite set of center frequency bins, E denotes the EVM value in dB and $\text{EVM}_{\text{up\_lim}}$ denotes the upper limits of the EVM value based on Table I. The constraints in the above formulations mean that the optimal center frequency only considers the cases that pass the EVM test. The search spaces mean that we calculate the EVM values over all MCS index values and all selected wireless optical CIRs. The countably finite sets of center frequency bins are defined as:

$$\mathcal{F}_1 \triangleq \{f|\ -28\text{dBr} \ \leq P_{\text{dBr}}(f) \leq -20\text{dBr}\}, \tag{4}$$

$$\mathcal{F}_2 \triangleq \{f|\ 80.5\text{MHz} \ \leq f \leq 160\text{MHz}\}, \tag{5}$$

where $P_{\text{dBr}}(f)$ denotes the power spectrum in dBr based on the spectral mask shown in Fig. 3. Our reference on choosing the range $[-28, -20]$ dBr is the noncontiguous transmission supported in the the IEEE 802.11ax. In the noncontiguous transmission, two 80 MHz channels are used, and the center frequencies are separated by 160 MHz. The two spectral masks are intersected at the region where the power spectrum is -28 dBr at $f_{\text{c}} = B$. Therefore, based on the noncontiguous transmission of the IEEE 802.11ax, we search in the range $[-28, -20]$ dBr expecting that there is an optimal center frequency such that $f_{\text{c}}^{*} < B$.

The difference between the three cases is that, in the first case, the optimal center frequency is defined for each signal bandwidth B. Meanwhile, in the second case, an optimal center frequency is calculated by considering all signal bandwidths. It will be shown in the next section that the optimal center frequency for the second case is not applicable for the system with the signal bandwidth of 160 MHz. The main reason for this is due to the optimal center frequency causing very severe spectral leakage. Therefore, the third case is defined to accommodate all signal bandwidths.

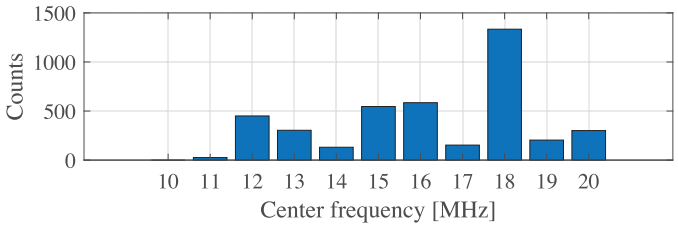

Fig. 7. Histograms showing that the optimal center frequency for the first case with the signal bandwidth of 20 MHz is 18 MHz.

TABLE II. Table of optimal center frequencies.

	Case 1				Case 2	Case 3
B (MHz)	20	40	80	160		
f_{c}^{*} (MHz)	18	38	72	112	81	112

For the first case and with the signal bandwidth of 20 MHz, the result is shown in Fig. 7. It is clear that most of the time, the smallest EVM is achieved with $f_{\text{c}} = 18$ MHz. Hence we can conclude that for $B = 20$ MHz, the optimal center frequency is 18 MHz. Results with other signal bandwidths are almost the same in the sense that there is a distinct center frequency at which most of the channels give the lowest EVM values. The results are summarized in Table II.

Unlike the results for the first case, the histograms of the center frequency for the second case are not distinct. That is, the center frequencies in the range around 80 MHz give the smallest EVM value, almost as many as that in the range around 160 MHz. The optimal center frequency in the range around 80 MHz is mostly caused by the system with $B = 20$, $B = 40$ and $B = 80$. Therefore, as can be seen in Fig. 8, the bins are denser in that range.

IV. Flatness Test

In this paper, a flatness test based on [15] will be used to measure the flatness of all selected channels in the reference models [18]. A channel is flat if deviations of all magnitudes of the channel estimation at all subcarriers are within predefined deviation limits. The deviations limits are taken from [15, Table 28-45] as depicted in Fig. 9. The limits have ± 4 dB and 4 or -6 dB ranges depending on the subcarrier index.

Based on [15], the flatness test should be carried out by using the binary phase-shift keying (BPSK) symbols with at least 20 packets. In addition, the training fields should also be used to estimate the frequency offset, detect the packets and estimate the channel.

Now, let us see an example as depicted in Fig. 10. This particular example is chosen based on the simulation results of the LC-optimized PHY with the adaptive bit loading as presented in [23]. It is concluded in [23] that using the previous

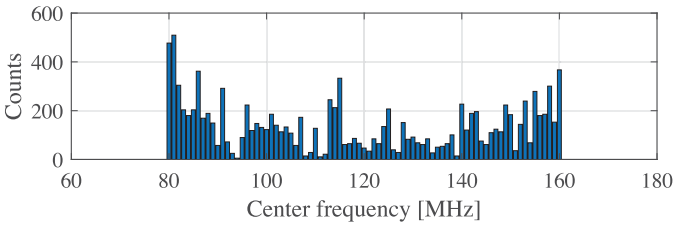

Fig. 8. Histograms showing that the optimal center frequency for the first case is 81 MHz.

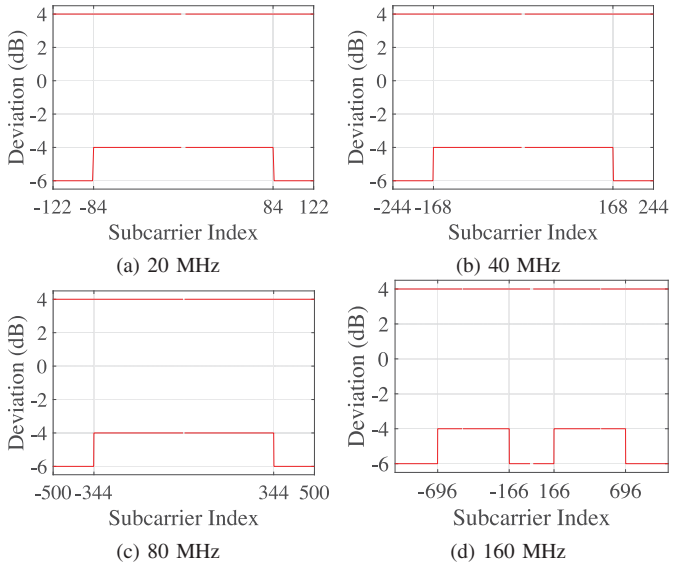

Fig. 9. Deviation limits for each signal bandwidth defined in [15, Table 28-45].

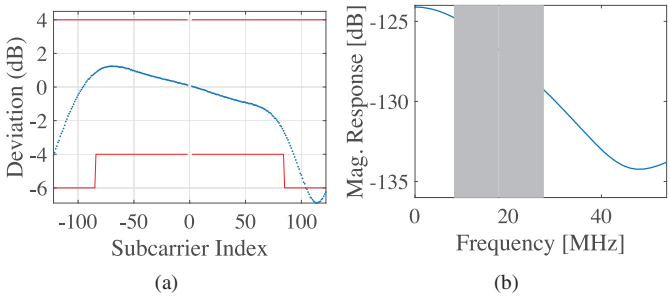

Fig. 10. (a) Flatness test for `'simulation scenario enterprise-conference room/individual cirs/optical cirs/S3/D1/Run1.mat'` and (b) the corresponding magnitude response and the location of the active subcarriers after the upconversion with $f_c = 18$ MHz.

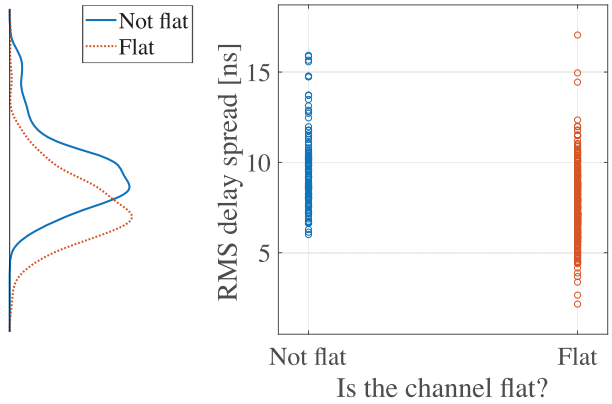

Fig. 11. The correlation between the root-mean-square delay spread and the flatness of the selected channels.

sample, the adaptive bit loading does not give a significant gain. Meanwhile, our flatness test indicates that the channel is not flat. Therefore, in this case, the deviation limits are pessimistic even though the maximum span of the deviation limits is 10 dB. In the next section, we will discuss the results of this test for all selected channels in the dataset.

V. Results and Discussion

Table III shows all results of the flatness test for both cases and all signal bandwidths. With $B = 20$ MHz, it has been shown that most channels are flat. The channels typically become less flatter as the signal bandwidth increases. It is worth noting here that with $B = 160$ MHz and $f_c = 81$ MHz, the received packet cannot be recovered due to errors in the training field, which are due to the spectral leakage. These errors mainly affect the frequency and timing offset detections.

Let us now look more deeply into the case with $B = 20$ MHz for each scenario as summarized in Table IV. It is obvious that given the number of possible availabilities of line-of-sight links in the geometries of LEDs and photodiodes (PDs) described in [19], the enterprise-conference room, hospital ward and the residential room have the channels that are predominantly flat. The LEDs in the industrial environment are placed on each side of a rotated cube, and the PDs are located across a 8.03 m $\times$ 9.45 m $\times$ 6.8 m room. Therefore, it is intuitive that most of the channels in the industrial environment are not flat.

For future work, it is also interesting to extend this study into experimental works. The reason behind this is that due to the observations made in [24, Fig. 6], which shows that as more orders of reflections are considered, the magnitude response of the non-line-of-sight channels becomes more fluctuated. This observation, in fact, can be also captured by investigating the delay spread of the channels. Fig. 11 shows the correlation between the channel flatness and the delay spread. This result supports our hypothesis that the received signals transmitted over flat channels are typically dominated by the signals coming from the low order reflections. The next question is now whether the high order reflections can really be received with the current off-the-shelf devices. In other words, is the signal coming from the high order reflections attenuated completely? If this is correct, it means that the LiFi channels are mostly flat in practice.

VI. Conclusions

We have discussed the flatness of the channels with regards to one of the proposals for the common mandatory PHY of the IEEE 802.11bb, i.e., using the existing PHY for LC. Our first approach was to determine the optimal center frequency that gives the best error performance. We highlighted the fact

TABLE III. Results of the flatness test to the selected channels.

	$B = 20$ MHz	$B = 40$ MHz	$B = 80$ MHz	$B = 160$ MHz
Case 1 (see Table II)	70.38%	17.56%	46.22%	14.5%
Case 2 ($f_c^* = 81$ MHz)	63.45%	30.25%	36.97%	N/A
Case 3 ($f_c^* = 112$ MHz)	62.82%	28.15%	15.34%	14.5%

The label 'N/A' (not applicable) indicates the fact that all received packets cannot be recovered mainly due to errors in the training fields.

TABLE IV. Results of the flatness test to the selected channels per scenario for $B = 20$ MHz.

	Case 1 ($f_c^* = 18$ MHz)	Case 2 ($f_c^* = 81$ MHz)	Case 3 ($f_c^* = 112$ MHz)
Enterprise	64 of 100 (64.00%)	69 of 100 (69.00%)	65 of 100 (65.00%)
Hospital ward	210 of 256 (82.03%)	173 of 256 (67.58%)	178 of 256 (69.53%)
Industrial	20 of 48 (41.67%)	20 of 48 (41.67%)	18 of 48 (37.50%)
Residential	41 of 72 (56.94%)	40 of 72 (55.56%)	38 of 72 (52.78%)

that there was a trade-off in choosing high center frequency, which is more resilient to the spectral leakage, and a low center frequency, which has a lower path loss. Table II summarized the results for the optimal center frequencies. Using these results, we applied the flatness test to all selected channels. Table III summarized the results for the flatness test. It could be concluded that with a signal bandwidth of 20 MHz, most of the channels are flat. Therefore, in this case, the existing PHY for LC will be more advantageous compared to the LC-optimized PHY.

VII. Acknowlegments

The work of A. Purwita was supported by Indonesian Endowment Fund for Education (LPDP). The work of H. Haas was supported by the Wolfson Foundation, the Engineering and Physical Sciences Research Council (EPSRC) under Established Career Fellowship grant EP/R007101/1.

References

[1] "Cisco visual networking index: Global mobile data traffic forecast update, 2017–2022," White Paper, Cisco, Feb. 2019.

[2] (2017, May) Status of IEEE 802.11 light communication TG. [Online]. Available: http://www.ieee802.org/11/Reports/tgbb_update.htm

[3] H. Haas, L. Yin, Y. Wang, and C. Chen, "What is LiFi?" *J. Lightw. Technol.*, vol. 34, no. 6, pp. 1533–1544, March 2016.

[4] L. Yin and H. Haas, "Physical-layer security in multiuser visible light communication networks," *IEEE J. Sel. Areas Commun.*, vol. 36, no. 1, pp. 162–174, Jan 2018.

[5] I. Stefan, H. Burchardt, and H. Haas, "Area spectral efficiency performance comparison between VLC and RF femtocell networks," in *2013 IEEE International Conference on Communications (ICC)*, Budapest, Hungary, June 2013, pp. 3825–3829.

[6] Y. Wang and H. Haas, "Dynamic load balancing with handover in hybrid Li-Fi and Wi-Fi networks," *J. Lightw. Technol.*, vol. 33, no. 22, pp. 4671–4682, Nov 2015.

[7] (2019, September) IEEE 802.15 WPAN™ 15.7 maintenance: Short-range optical wireless communications task group (TG 7m). [Online]. Available: http://www.ieee802.org/15/pub/IEEE%20802_15%20WPAN%2015_7%20Revision1%20Task%20Group.htm

[8] (2019, September) IEEE 802.15 WPAN™ task group 13 (TG13) multi-gigabit/s optical wireless communications. [Online]. Available: http://www.ieee802.org/15/pub/TG13.html

[9] "High-speed indoor visible light communication transceiver – system architecture, physical layer and data link layer specification," *Rec. ITU-T G.9991, International Telecommunications Union*, 2019.

[10] V. Jungnickel, V. Pohl, S. Nonnig, and C. von Helmolt, "A physical model of the wireless infrared communication channel," *IEEE IEEE J. Sel. Areas Commun.*, vol. 20, no. 3, pp. 631–640, April 2002.

[11] S. Shao, A. Khreishah, M. B. Rahaim, H. Elgala, M. Ayyash, T. D. C. Little, and J. Wu, "An indoor hybrid WiFi-VLC internet access system," in *2014 IEEE 11th International Conference on Mobile Ad Hoc and Sensor Systems*, Philadelphia, PA, USA, Oct 2014, pp. 569–574.

[12] Yuanquan Wang, Yufeng Shao, Huiliang Shang, Xiaoyuan Lu, Yiguang Wang, Jianjun Yu, and Nan Chi, "875-Mb/s asynchronous bi-directional 64QAM-OFDM SCM-WDM transmission over RGB-LED-based visible light communication system," in *2013 OFC/NFOEC*, Anaheim, CA, USA, March 2013, pp. 1–3.

[13] R. Mesleh, H. Elgala, and H. Haas, "On the performance of different OFDM based optical wireless communication systems," *IEEE J. Opt. Commun. Netw.*, vol. 3, no. 8, pp. 620–628, August 2011.

[14] A. Zeshan and T. Baykas, "Performance analysis of VLC based on 802.11ac frame structure," *IEEE Communications Letters*, vol. 23, no. 9, pp. 1560–1563, Sep. 2019.

[15] "IEEE draft standard for information technology – telecommunications and information exchange between systems local and metropolitan area networks – specific requirements part 11: Wireless LAN medium access control (MAC) and physical layer (PHY) specifications amendment enhancements for high efficiency WLAN," *IEEE P802.11ax/D3.0, June 2018*, pp. 1–682, July 2018.

[16] K. L. Bober, V. Jungnickel, M. Hinrichs, and N. Serafimofski. (2019, May) TGbb: Evaluation methodology for PHY and MAC proposals. [Online]. Available: https://mentor.ieee.org/802.11/dcn/19/11-19-0187-04-00bb-evaluation-methodology-for-phy-and-mac-proposals.docx

[17] M. Hinrichs, J. Hilt, P. Hellwig, V. Jungnickel, and K. L. Bober. (2019, January) IEEE 802.11 TGbb Task Group on Light Communications: Optical Frontend Model. [Online]. Available: https://mentor.ieee.org/802.11/dcn/19/11-19-0087-01-00bb-optical-frontend-model-for-phy-simulation.docx

[18] M. Uysal, F. Miramirkhani, T. Baykas, and K. Qaraqe. (2018, November) CIRs of IEEE 802.11bb reference channel models for indoor environments. [Online]. Available: https://mentor.ieee.org/802.11/dcn/18/11-18-1603-01-00bb-cirs-of-ieee-802-11bb-reference-channel-models.zip

[19] ——. (2018, November) IEEE 802.11bb reference channel models for indoor environments. [Online]. Available: https://mentor.ieee.org/802.11/dcn/18/11-18-1582-04-00bb-ieee-802-11bb-reference-channel-models-for-indoor-environments.pdf

[20] N. Serafimofski, T. Weszely, Z. Zeng, and H. Haas. (2019, July) Simulation results for 802.11a PHY in LC. [Online]. Available: https://mentor.ieee.org/802.11/dcn/19/11-19-1224-01-00bb-simulation-results-for-802-11a-phy-in-lc.ppt

[21] J. M. Kahn and J. R. Barry, "Wireless infrared communications," *Proceedings of the IEEE*, vol. 85, no. 2, pp. 265–298, Feb 1997.

[22] M. S. Islim, S. Videv, M. Safari, E. Xie, J. J. D. McKendry, E. Gu, M. D. Dawson, and H. Haas, "The impact of solar irradiance on visible light communications," *J. Lightw. Technol.*, vol. 36, no. 12, pp. 2376–2386, June 2018.

[23] M. Hinrichs, K. L. Bober, V. Jungnickel, and R. Fischer. (2019, September) Simulation results with bit-loading for the lc-optimized phy. [Online]. Available: https://mentor.ieee.org/802.11/dcn/19/11-19-1566-03-00bb-simulation-results-with-bit-loading-for-the-lc-optimized-phy.pptx

[24] H. Schulze, "Frequency-domain simulation of the indoor wireless optical communication channel," *IEEE Trans. Commun.*, vol. 64, no. 6, pp. 2551–2562, June 2016.